

City Research Online

City St George's, University of London

Citation: Papoutsakis, A. & Gavaises, M. (2020). A model for the investigation of the second-order structure of caustic formations in dispersed flows. Journal of Fluid Mechanics, 892, A4. doi: 10.1017/jfm.2020.176

This is the accepted version of the paper.

This version of the publication may differ from the final published version. To cite this item please consult the publisher's version.

Permanent repository link: https://openaccess.city.ac.uk/id/eprint/24087/

Link to published version: https://doi.org/10.1017/jfm.2020.176

Copyright and Reuse: Copyright and Moral Rights remain with the author(s) and/or copyright holders. Copies of full items can be used for personal research or study, educational, or not-for-profit purposes without prior permission or charge, unless otherwise indicated, provided that the authors, title and full bibliographic details are credited, a hyperlink and/or URL is given for the original metadata page and the content is not changed in any way. For full details of reuse please refer to City Research Online policy.

City Research Online: http://openaccess.city.ac.uk/ publications@citystgeorges.ac.uk

A model for the investigation of the "second–order" structure of caustic formations in dispersed flows

Andreas Papoutsakis [1]†, and M. Gavaises [1]

[1]School of Mathematics, Computer Science and Engineering, Department of Mechanical Engineering and Aeronautics, City, University of London, EC1V 0HB, London, UK.

(Received xx; revised xx; accepted xx)

The formation of caustics by inertial particles is distinctive of dispersed flows. Their pressureless nature allows crossing trajectories resulting in singularities that cannot be captured accurately by standard Lagrangian approaches due to their fine spatial scale. A promising method for the investigation of caustics is the Osiptsov method or Fully Lagrangian Approach (FLA). FLA has the advantage to identify caustics, but its applicability is hindered by the occurrence of singularities. We present an original robust framework based on the FLA that provides an explicit expression of the dispersed phase structure that does not degenerate in the vicinity of caustics, using a single representative particle. The FLA is extended to account for the Hessian of the Dispersed Continuum (DC). It demonstrates the integrability of the FLA number density and allows for the calculation of the number density on a given length scale, retaining the functionality of the FLA.

Number density models based on the "second–order" representation of the DC and on the one–dimensional structure of the particle distribution, that account for the anisotropy of the DC on caustics, are derived and applied for analytical flows. The number density is linked to a finite length scale, needed for the introduction of the FLA to spatially filtered flow fields. Finally, the method is used for the calculation of the inter-particle separation on caustics. The identification of the structure of caustics presented in this work paves the way to a robust understanding of the mechanisms of particle accumulation.

Key words: Hessian; Fully Lagrangian Approach; Particles; Droplets; Caustics.

1. Introduction

Inertial droplets and/or particles in dispersed flows exhibit compression regions and intersecting trajectories which result in caustic formations (Crisanti *et al.* 1992; Meneguz & Reeks 2011). Caustic formations (Caustics) are zones of high concentration and their intensity is important to a great variety of environmental, biological, engineering and consmological (Tomita & Den 1986) applications. For example, the behaviour of microorganisms is affected by the accumulation of nutrients (Vogel 1994) and the migration of sea organisms and coral colonies is governed by the formation of caustics created by sea currents (Serrano *et al.* 2016). Sea currents and weather systems result to the local accumulation of pollutants, plastic debris (Lebreton *et al.* 2018) and aerosols (Knight

† Email address for correspondence: andreas.papoutsakis@city.ac.uk

2012). Also, environmental pollution (Bell *et al.* 2007), the impact of radioactive particles (Thomas & Martin 1986) and the potency of spray delivered medication (Rygg *et al.* 2016), are strongly dependent on the formation of such accumulation regions (Sazhin 2014). In internal combustion engines the vortical structures of the in-cylinder carrier phase flow field induce accumulation regions of the spray droplets during fuel injection, affecting the local stoichiometry of the mixture (Papoutsakis *et al.* 2018*b*). Caustics in cumulus clouds has been reported to affect the patterns of rain (Ravichandran & Govindarajan 2015) due to the sling effect of the vortical structures (Wilkinson *et al.* 2007).

In the general case particles interact only due to collisions (Marble 1970), for a diluted system of dispersed flows (Kasbaoui *et al.* 2019), however, interparticle collisions can be neglected (Williams 1958; Bec 2003), resulting to a pressureless continuum model (Kasbaoui *et al.* 2019; Tomita & Den 1986). The pressureless nature of dispersed flows allows the crossing of particle trajectories and results in caustic structures which are compression regions formed by the undulation of the dispersed phase. Standard Lagrangian Approaches (LA) use a representative sub-set of the actual number of physical particles. Instances of caustics are singularities that cannot be captured accurately since they consist of a large concentration of particles focused in a small length scale, and demand a prohibitive number of representative Lagrangian particles to be described (Healy & Young 2005). In Papoutsakis *et al.* (2018*a*) it was shown that the number density calculated with LA could not converge even for 10^6 representative particles per direction for a simple one–dimensional flow field.

The Fully Lagrangian Approach, (standard FLA or Osiptsov method) (Osiptsov 1984), offers an efficient alternative by treating the particulate phase as a continuum. FLA solves the particle number conservation equation in Lagrangian form along a single trajectory and provides the equations for the components of the Jacobi matrix of transformation from the Eulerian to the Lagrangian coordinates. This is essentially a method of characteristics and can deal with complex cases such as intersecting particle trajectories and caustics and presents unique properties in capturing the occurrence of accumulation regions. FLA utilises the definition for the density ρ for a deformed continuum, by introducing the Jacobian matrix determinant $|\boldsymbol{J}|$ (i.e. $\rho_0 = |\boldsymbol{J}|\rho$) as it is used in solid mechanics (Healy & Young 2005). Although a dispersed phase consists of scattered individual entities, a Dispersed Continuum (DC) can be defined. This implies continuous fields for the particle number density and the particle velocity. Of course, the limit of the continuum assumption must be respected. Under the DC assumption, particles transport remaining attached to the Lagrangian DC, which is following the motion of the particles. Due to the absence of pressure in dispersed flows (in contrast to solid mechanics) the continuum can intersect itself, creating overlapping folds, and particle collisions may occur among particles that are attached to overlapping folds (Ravichandran & Govindarajan 2015). The folds are areas of negative Jacobian, something that is not observed in continuum mechanics. It must be stressed here that even if pressure due to particle collisions is accounted for, dispersed flows do present intersecting trajectories. In the process of the creation of the folds for the DC, areas of zero Jacobian will emerge. The loci of zero Jacobian are characterised by infinite number density thus identifying caustic formations.

The efficiency and the modelling capabilities of the FLA in identifying the spatial structure of caustics was demonstrated in Healy & Young (2005) and in Ijzermans *et al.* (2009). The introduction of the FLA into the study of turbulent flows (Meneguz & Reeks 2011) and (Picciotto *et al.* 2005) resulted in the identification and analysis of spatial structures of the dispersed phase distribution using the moments of concentration. Ac-

cording to Picciotto *et al.* (2005) FLA has great potential for reductions in computational time compared with the standard Eulerian–Lagrangian approach (LA) and provides a sound mathematical framework for interpreting the physics of particulate flows.

However, the occurrence of singularities in FLA hinders the applicability of the method. Singularities pose a serious controversy in the interpretation of the FLA results. In literature, singularities are treated either by clipping large values of density (see Ducasse & Pumir (2009)) or by introducing the concept of number density moments (i.e $\overline{n^a} = \left\langle |\boldsymbol{J}|^{1-a} \right\rangle$ (Ijzermans *et al.* 2010)) which was used for the analysis of spatial structures of the dispersed phase in turbulent flows. The zeroth moment has been used in Meneguz & Reeks (2011) and in Ijzermans *et al.* (2010) for the evaluation of an averaged number density. This approach, however, cancels out the effect of the continuum deformation by multiplying the FLA density $1/|\boldsymbol{J}|$ by $|\boldsymbol{J}|$, and results to the transformation of the FLA to a standard Lagrangian approach. The averaged number density for higher moments gives non-physical values that reach to the order of 10^{10} (Meneguz & Reeks 2011; Ijzermans *et al.* 2010). The actual values of these peaks are coincidental and are mostly related to the temporal resolution of the numerical integration during the instances of sign change of the Jacobian. A turbulent diffusion model was introduced for the "first–order" FLA in Papoutsakis *et al.* (2018*a*). The extended "first–order" FLA was implemented and assessed for Direct Numerical Simulations (DNS) for Stokesian droplets in Homogeneous Isotropic Turbulence (HIT) using the standard LA. and was shown that the FLA singularities infect the spatially averaged result. Thus, it becomes essential that the FLA number density should be interpreted alongside with the spatial structure of the DC "DC-structure" and must be connected to a length scale within a robust mathematical framework.

In this work we present an integrated framework that lifts the ambiguity of the FLA number density definition. We understand that because the FLA number density is defined for an infinitesimally small volume resulting to a point-wise density it results to singularities. Our approach is based on the observation that a) the particulate phase and the DC are not identical concepts, instead the particles are sporadically attached to the DC at finite inter-particle distances, and b) the deformation of the DC cannot be captured by linear expressions, thus it is necessary to account for the curvature of its structure. The model is based on representing the dispersed phase as a local approximation for the spatial "DC-structure", using the Jacobian and the Hessian of the transformation of the DC from the Lagrangian to the Eulerian coordinates. Choosing a first–order representation we obtain the standard FLA method, in a formulation that highlights the modelling capabilities and shortcomings of the standard FLA as a first–order approximation of the "DC-structure". In a "second–order" expression of the "DC-structure" we obtain the derivation of an original "second–order" model, which provides the averaged FLA number density on a finite volume either by utilising the modelled second–order structure or by assuming a simplified one–dimensional structure on a primary direction.

Specifically, we present a model for the multi-dimensional structure of a dispersed phase based on the Jacobian and the Hessian of the transformation from the Lagrangian to the Eulerian coordinates. The Hessian and the Jacobian matrices are obtained by solving an initial value problem in multiple dimensions presented here, using a derivation that is in line with the Osiptsov method. Number density expressions are derived either from the 3D structure or assuming a one–dimensional structure which is then projected along a primary direction. An algebraic model for the number density is derived and can be used for a reduced model of the number density and the "DC-structure" by rotating the coordinate system along a primary direction. Thus, the derivation of all the elements needed for the application of the method to engineering problems is presented. The results

inferred from the different approaches presented in this work are compared with the results stemming from the direct integration of individual particles. For the comparison of the two approaches (i.e. the LA and the FLA), the anisotropy of the length scales parallel and the perpendicular to the caustic front are accounted for. In our study the proposed methodology is used for the investigation of caustic events for different Stokes numbers. Finally, the pressureless continuum assumption on a caustic is investigated by calculating the length scales of the average inter-particle separation.

In Section 2, a representation of the local "DC-structure" based on the Taylor expansion of the DC coordinates is presented. This approach lays the foundations of the "second–order" FLA and also provides an insightful representation of the standard first–order FLA. In addition, the initial value problem for the calculation of the Hessian matrix in multi–dimensional problems is derived. In Section 3 the local "DC-structure" for a Stokesian dispersed phase convected by Taylor vortices is calculated using direct integration of a lattice of particles and is compared to the result from the first and the "second–order" representations. In Section 4, the number density on a finite volume is defined. The results from the calculation of the number density, on multiple dimensions assuming a "second–order" one–dimensional "DC-structure" based on the Hessian of the Lagrangian transformation, (i.e. the curvature of the deformed DC) are also presented. In the next sections the effect of the Stokes number on the structure of caustic formations is discussed.

2. Second order Fully Lagrangian Approach

FLA provides a method to calculate the number density for a DC along the trajectory of a particle. A particle trajectory is the evolution of the position $\mathbf{x}^p(t)$ of a particle with Lagrangian coordinate $(\mathbf{x}_0^p, t)$ in time t. The vector $\mathbf{x}_0^p$ is the initial position of the particle at time $t = 0$. The calculation of the number density in the FLA context is based on the transformation of an infinitesimal volume V_L defined on the initial Lagrangian coordinates $\mathbf{x}_0^p$ to the deformed Lagrangian volume at t. The compression or expansion of V_L is quantified by the Jacobian of the transformation defined as $J_{ij} = \frac{\partial x_i^p}{\partial x_{j,0}^p}$, where $x_{j,0}^p$ is the Lagrangian coordinate and x_j^p refers to the particle p and is equivalent with the Eulerian coordinate x_j. In the FLA the number density n^p along a trajectory, non–dimensionalised by the initial number density n_0^p is:

$$n^p = \frac{1}{J}\,, \tag{2.1}$$

where J is the determinant of the Jacobian matrix $\mathbf{J}$. When J tends to zero the number density tends to infinity, thus signifying the occurrence of a caustic. The occurrence of singularities is due to the point-wise definition of the number density in the FLA framework $n^p = \frac{\lim_{V\to 0} N/V}{n_0^p}$. Since the particles are dispersed and are characterised by a minimum finite separation scale, this point-wise density corresponds to the "DC-structure" rather than the particulate phase itself.

In order to investigate the integrability of this number density on a caustic, we need to focus in the Eulerian spatial structure of the DC. This can be revealed by representing the dispersed phase distribution in the vicinity of a particle trajectory using the coordinates of a particle $\mathbf{x}^p(\mathbf{x}_0^p + \boldsymbol{\delta}, t)$ neighbouring to $\mathbf{x}^p(\mathbf{x}_0^p, t)$, where the vector $\boldsymbol{\delta}$ is the initial separation of the particles. Assuming a Taylor expansion for the distribution of the

neighbours of $\mathbf{x}^p(\mathbf{x}_0^p)$ at a time t, the "DC-structure" can be represented as:

$$\mathbf{x}^p(\mathbf{x}_0^p + \boldsymbol{\delta}) = \mathbf{x}^p(\mathbf{x}_0^p) + \frac{\partial \mathbf{x}^p}{\partial x_{j,0}^p}\delta_j + \frac{1}{2}\frac{\partial^2 \mathbf{x}^p}{\partial x_{j,0}^p \partial x_{k,0}^p}\delta_j\delta_k + \dots \ . \tag{2.2}$$

Employing a linear expansion in three dimensions, the position $\mathbf{x} + \boldsymbol{\epsilon}$ of the particle $(\mathbf{x}_0 + \boldsymbol{\delta}, t)$ in the vicinity of $(\mathbf{x}_0, t)$ is expressed as:

$$\epsilon_i(\boldsymbol{\delta}) = J_{ij}\delta_j \ , \tag{2.3}$$

where $\boldsymbol{\delta} = \mathbf{x}_0 - \mathbf{x}_0^p$ is the displacement vector of a particle at $t = 0$ and $\boldsymbol{\epsilon} = \mathbf{x} - \mathbf{x}^p$ is the displacement vector of the same particle at t. Vector indices i, j correspond to vector components and summation is assumed among the repeated indices. It can be observed that the first–order spatial derivatives in 2.2 correspond to the Jacobian matrix, thus, 2.3 can be perceived as the expression of the "DC-structure" in the standard FLA framework. In the following Sections it will be shown that in the case of caustic formations (i.e. $J = 0$) the expression 2.3 results in an undefined structure where all particles collapse on a plane.

The linear representation of the dispersed phase degenerates when $J = 0$, however, this is not the case for the actual distribution of the particles. The expression 2.2 can be extended to account for a "second–order" description of the DC which provides the "DC-structure", even for small values of J, as:

$$\epsilon_i(\delta) = J_{ij}\delta_j + \frac{1}{2}H_{ijk}\delta_j\delta_k \ , \tag{2.4}$$

where H_i is a two dimensional matrix, for each Cartesian coordinate i, and is defined as $H_{ijk} = \frac{\partial^2 x_i^p}{\partial x_{j,0}^p \partial x_{k,0}^p}$. H_i corresponds to the Hessian matrix of the transformation from the Eulerian to the Lagrangian coordinates.

For a particulate flow field with characteristic length L and a characteristic velocity U we can define the non–dimensional carrier phase velocity field $\mathbf{U}$ and the induced particulate velocity $\mathbf{V}$. In the classical FLA, the Jacobian $J_{ij} = \frac{\partial x_i^p}{\partial x_{j,0}^p}$ is calculated by introducing the auxiliary variable ω_{ij}, which is the time derivative of the Jacobian:

$$\omega_{ij} = \frac{\partial J_{ij}}{\partial t} = \frac{\partial}{\partial t}\left(\frac{\partial x_i^p}{\partial x_{j,0}^p}\right) = \frac{\partial V_i}{\partial x_{j,0}^p} \ . \tag{2.5}$$

Although the calculation of the Jacobian can be extended for non-Stokesian particles (Papoutsakis *et al.* 2018*a*) we will assume a Stokesian drag force in our analysis. In this case the non—dimensional acceleration of the particles is: $\ddot{x}_i = \frac{\partial V_i}{\partial t} = \frac{1}{St}(U_i - V_i)$ where St$= t_p/T$ is the Stokes number of the flow (Sazhin 2014), t_p is the particle relaxation time and $T = L/U$ is the characteristic time. Thus, following Osiptsov (1984), the initial value problem for ω_{ij} is obtained as:

$$\frac{\partial \omega_{ij}}{\partial t} = \frac{\partial}{\partial x_{j,0}^p}\left(\frac{\partial V_i}{\partial t}\right) = \frac{1}{St}\left(\frac{\partial x_m^p}{\partial x_{j,0}^p}\frac{\partial U_i}{\partial x_m} - \frac{\partial V_i}{\partial x_{j,0}}\right) = \frac{1}{St}\left(J_{mj}\frac{\partial U_i}{\partial x_m} - \omega_{ij}\right) \ , \tag{2.6}$$

where addition is assumed among the terms with index m. For the derivation of 2.6 the chain rule $\frac{\partial(\cdot)}{\partial x_{i,0}} = \frac{\partial(\cdot)}{\partial x_i}\frac{\partial x_i^p}{\partial x_{i,0}^p}$ is used with $x_i^p \equiv x_i$. The equation 2.6 is integrated using the initial condition $\omega_{ij} = \left|_{t=0}\frac{\partial V_i}{\partial x_j}\right.$ stemming from 2.5.

For the derivation of an expression for the Hessian H_{ijk}, needed for the "second–order" FLA in three dimensions, the auxiliary variable ψ_{ijk} is inroduced, defined as the time

derivative of the Hessian:

$$\psi_{ijk} = \frac{\partial H_{ijk}}{\partial t} \ . \tag{2.7}$$

The Hessian time rate ψ_{ijk} can be expressed as the spatial derivative of the rate of the Jacobian ω_{ij} over the Lagrangian coordinate $x^p_{k,0}$ as:

$$\frac{\partial \psi_{ijk}}{\partial t} = \frac{\partial}{\partial t}\left(\frac{\partial \omega_{ij}}{\partial x^p_{k,0}}\right) = \frac{\partial}{\partial x^p_{k,0}}\left(\frac{\partial \omega_{ij}}{\partial t}\right) = \frac{\partial}{\partial x^p_{k,0}}\left(\frac{1}{St}\left(J_{mj}\frac{\partial U_i}{\partial x_m} - \omega_{ij}\right)\right) \ . \tag{2.8}$$

Using the chain rule as in 2.6 we finally obtain an expression for the Hessian time rate:

$$\frac{\partial \psi_{ijk}}{\partial t} = \frac{1}{St}\left(H_{mjk}\frac{\partial U_i}{\partial x_m} + J_{mj}J_{nk}\frac{\partial^2 U_i}{\partial x_m \partial x_n} - \psi_{ijk}\right) \ , \tag{2.9}$$

where addition is assumed among the terms with indices m and n. For $t = 0$ the Lagrangian derivative coincides with the Eulerian derivative, thus, the initial condition for ψ is $\psi_{ijk}(t=0) = \frac{\partial^2 V_i}{\partial x_j \partial x_k}$. Assuming that at $t = 0$ the DC is not deformed, the expression $H(t=0) = 0$ can be used as the initial value for H_{ijk}.

The initial value problem for the calculation of the Hessian and the Jacobian under the "second–order" FLA concept as described by the equations 2.5, 2.6, 2.7 and 2.9 can be summarised by the non-linear first–order differential system:

$$\frac{\partial}{\partial t}\begin{bmatrix} J_{ij} \\ \omega_{ij} \\ H_{ijk} \\ \psi_{ijk} \end{bmatrix} = \begin{bmatrix} \omega_{ij} \\ \frac{1}{St}\left(\frac{\partial U_i}{\partial x_m}J_{mj} - \omega_{ij}\right) \\ \psi_{ijk} \\ \frac{1}{St}\left(H_{mjk}\frac{\partial U_i}{\partial x_m} + J_{mj}J_{nk}\frac{\partial^2 U_i}{\partial x_m \partial x_n} - \psi_{ijk}\right) \end{bmatrix}, \quad \begin{bmatrix} J_{ij} \\ \omega_{ij} \\ H_{ijk} \\ \psi_{ijk} \end{bmatrix}_{t=0} = \begin{bmatrix} 1 \\ \frac{\partial V_i}{\partial x_j} \\ 0 \\ \frac{\partial^2 V_i}{\partial x_j \partial x_k} \end{bmatrix}, \tag{2.10}$$

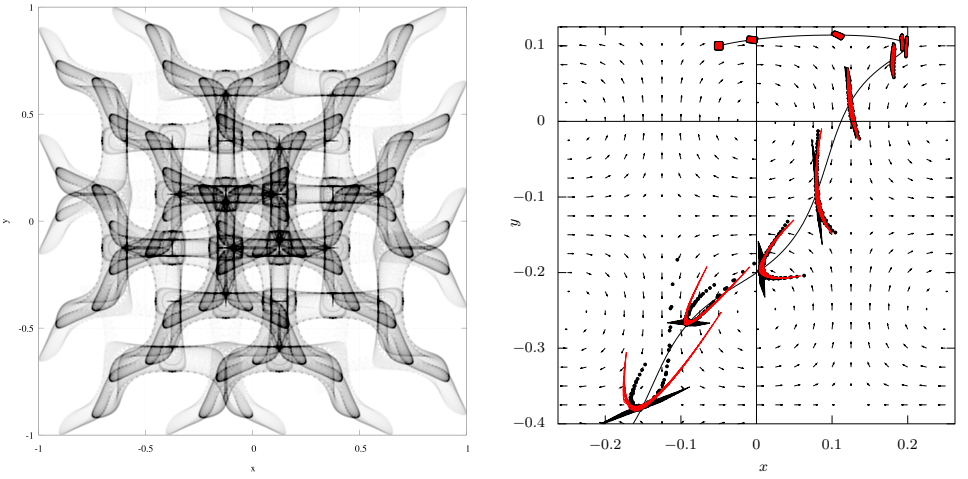
where addition is assumed among the terms $m = 1 \ldots 3$ and $n = 1 \ldots 3$. The system of equations 2.10 is integrated with an appropriate numerical method (e.g. Runge–Kutta) and provides the entries of the Jacobian and the Hessian matrices along a particle trajectory.

From the Equation 2.10 it can be inferred that for a linear converging flow field with $U(y) = -y$, $\partial^2 U/\partial x^2 = 0$, the Hessian is zero and at the focal point y=0 the number density will be genuinely infinite (Morse point) as all particles will meet at the same location. As the curvature of the carrier phase field becomes non-zero, the Hessian will be generally non-zero ($H \neq 0$) and the number density would be finite.

3. Second order structure of a Stokesian dispersed phase in a periodic two–dimensional array of Taylor vortices

In this section we present the result from a Kinematic Simulation (KS) (see Monchaux *et al.* (2012)) of the structure of a DC that conveys in a carrier phase flow field that consists of a periodic distribution of two–dimensional stationary Taylor vortices. Similar synthetic flow fields have been used in the analysis of Crisanti *et al.* (1992). The dispersed phase consists of 500×500 individual particles with Stokes number $St = 0.1$. Initially, the particles are uniformly distributed in a square with size L. The carrier phase flow field $\mathbf{U} = (U_1, U_2)$ is an incompressible synthetic flow field defined by the analytical expression:

$$U_1(x,y) = U_0 \cos(2\pi n x)\sin(2\pi n y), \ \ \textit{and}\ U_2(x,y) = -U_0 \sin(2\pi n x)\cos(2\pi n y) \ , \tag{3.1}$$



(**a**) (**b**)

Figure 1: **(a)** Distribution of particles at $t = 0.4$. **(b)** Solid black line: Trajectory of the reference particle from $t = 0$ to $t > 0.45$ as calculated by direct integration of the particle equation of motion assuming Stokes particles. Black dots: Distribution of the neighbouring particles calculated by direct integration of the particle equation of motion. Red lines: Particle distribution inferred from the "second–order" description of the DC structure. Black lines: Particle distribution inferred from the first–order description of the "DC-structure". The particle distributions are shown at regular intervals $t = 0.00, 0.05, 0.10, 0.15, \ldots, 0.45$ and at $t = 0.1655$. Instance $t = 0.1655$ corresponds to a caustic formation. The vector field represents the carrier phase velocity field.

where x and y are the dimensionless coordinates, normalised by L. The velocity amplitude U_0, non–dimensionalised by U, is equal to $U_0 = 5$ and the wavenumber is $n = 2$. The result of the particles distribution at time $t = 0.4$ as calculated by integrating the equation of motion $\ddot{\mathbf{x}}^p = (\mathbf{U} - \mathbf{V})/\mathrm{St}$, is shown in figure 1(**a**). The expression 3.1 provides the exact values of the velocity field and its spatial derivatives at any point of the Eulerian domain, needed for the integration of the initial value problem described by the equation 2.10, as well as for the solution of the equation of motion. The equation of motion and the initial value problem 2.10 are both integrated using a fourth order Runge Kutta method.

In figure 1(**a**) the position of each particle is shown by transparent black coloured circles and the particle agglomeration is identified by the dark filaments shown in this figure. The trajectory of a single particle initially located at $(-0.05, 0.1)$ is shown in figure 1(**b**). The distribution of 80 particles neighbouring to the reference particle and arranged in a rectilinear lattice of 9×9 particles with a initial separation $|\boldsymbol{\delta}| = 0.0005$ is also shown in figure 1 (**b**). Their trajectories are calculated by direct integration and they are presented as black dots at regular intervals. The black and red lines in figure 1(**b**) represent the local "DC-structure" as calculated by 2.3 and 2.4 which correspond to the first and "second–order" representation of the DC structure, using the initial separation vector $|\boldsymbol{\delta}|$ for each neighbouring particle. The components of the Jacobian and the Hessian matrices needed by 2.3 and 2.4 are calculated by the initial value problem 2.10, derived in the previous section.

4. Calculation of the particle number density

In this section a method for calculating a number density defined at a finite length–scale is presented. This number density is calculated from the first and the "second–order" model for the DC structure. An analytical model for the number density, assuming a one–dimensional "second–order" representation of the DC is also derived. In the figures 2(**a-d**) we focus in the dispersed phase for four instances. From the figures 2(**a-d**) and from the figure 1(**b**) it can be inferred that the "second–order" FLA can provide a satisfactory approximation of the DC structure even at significant distances from the reference trajectory. The method not only captures the compression of the DC but also resolves the complex non-isotropic "DC-structure" even when this collapses to a caustic filament (see figure 2(**b**)).

In conjunction with the point-wise density n^p, a number density $\hat{n}^p$ defined at a finite length–scale can be inferred from the "DC-structure" for each one of the three above mentioned methods as:

$$\hat{n}^p = \frac{1}{S_t} \,, \tag{4.1}$$

where $\hat{n}^p$ has been normalised by the initial number density n_0^p, and S_t is the surface of the lattice defined by the eight particles closest to the reference particle p at t normalised by the initial surface of the lattice S_0. The number density $\hat{n}^p$ in 4.1 is defined at a finite length–scale $\Delta \sim \sqrt{S_t}$. Figure 2(**b**) corresponds to the instance $t = 0.1655$, for which the particles agglomerate to a caustic. In figure 2(**b**) it can be observed that the first–order structure as provided by 2.3 and indicated by the black line mesh, collapses to a single line with $S_t = 0$, since $J_{11}J_{22} - J_{12}J_{21} = 0$. This results to an infinite number density $n = 1/J$. The rationale behind the occurrence of infinite number densities in the standard FLA lays on the fact that the first–order approach provides a point-wise number density (i.e. the number density that corresponds to an infinitesimally small volume) and is based on the local DC deformation. This behaviour is nonphysical because number density should be defined for a finite length–scale. The particulate phase is dispersed, thus the definition of a point-wise definition breaches the continuity assumption.

For the derivation of an analytical model for a number density defined at a finite length–scale, we can assume a simplified one–dimensional "second–order" "DC-structure" for a caustic formation. This assumption can be based on the observation that these formations appear as filaments with a one–dimensional structure along a preferential direction (see figure 1). A coordinate system δ, ϵ attached to the reference particle and perpendicular to the filament can be chosen so that J and H are both positive (see figure 3). Thus a one–dimensional "DC-structure" can be expressed as $\epsilon(\delta) = J\delta + 0.5H\delta^2$ (or as $\delta(\epsilon) = \frac{-J+\sqrt{J^2+2H\epsilon}}{H}$, where the binomial root closer to the reference point is chosen).

The solid line in figure 3 depicts the schematic representation of a one–dimensional DC. The DC is presented in terms of the Lagrangian x_0 and Eulerian x coordinate. In the specific example the DC has folded, thus it is multiply defined for a part of the Eulerian field. The local coordinate ϵ corresponds to the Eulerian coordinate $\mathbf{x}$ and the local coordinate δ corresponds to the Lagrangian coordinate $\mathbf{x}_0$. The averaged point-wise number density $1/J = d\delta/d\epsilon$ for an interval $[-R_\epsilon, R_\epsilon]$ with length $L = 2R_\epsilon$ at the proximity of the point **A** shown in the figure 3 (scenario **A**) is:

$$\hat{n}^p = \frac{1}{2R_\epsilon} \int_{-R_\epsilon}^{R_\epsilon} \frac{d\delta}{d\epsilon} d\epsilon = \frac{|\delta(R_\epsilon) - \delta(-R_\epsilon)|}{2R_\epsilon} \,, \tag{4.2}$$

where $\delta(\pm R_\epsilon) = (-J + \sqrt{J^2 \pm 2HR_\epsilon})/H$.

For the lower bound of the interval $[-R_\epsilon, R_\epsilon]$ (i.e. $\epsilon = -R_\epsilon$) the equation $\epsilon(\delta) = -R_\epsilon$

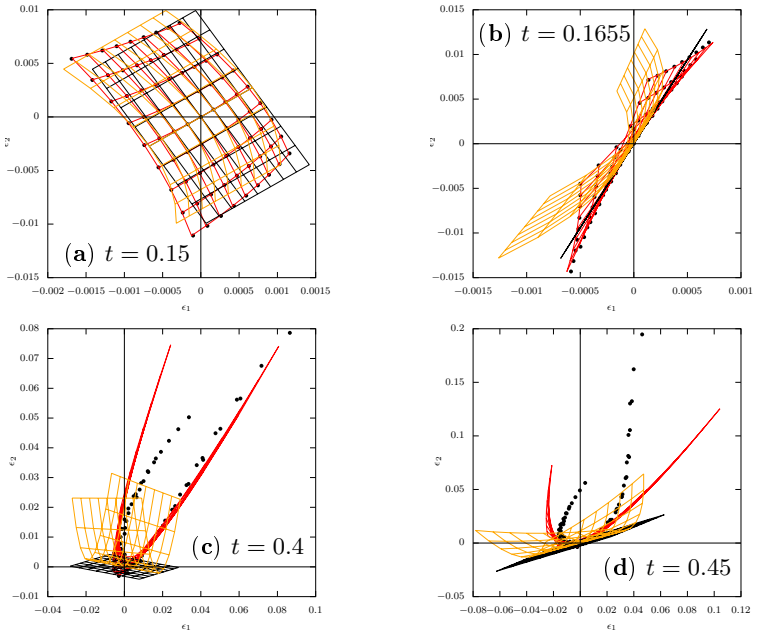


Figure 2: Black dots: Distribution of particles neighbouring to the reference trajectory. Red lines: Particle distribution inferred from the "second–order" description of the "DC-structure". Black lines: Particle distribution inferred from the first–order description of the "DC-structure". Orange lines: Particle distribution inferred from the first–order one–dimensional description of the "DC-structure". Figure (b) corresponds to a caustic formation, where the lattice that corresponds to the first–order representation (shown with black grid lines) has degenerated to a straight line.

will not have a root if $J^2 < 2HR_\epsilon$ (see scenario **B** figure 3(**a**)). This scenario occurs when the caustic occurs within the Eulerian interval $[-R_\epsilon, R_\epsilon]$ and there is a minimum $\epsilon = J\delta + 0.5H\delta^2$, $\epsilon_{min} = -\frac{J^2}{2H} > -R_\epsilon$ for $\delta_{min} = \delta(\epsilon_{min}) = -J/H$. In this case the integration is done along the interval $[\epsilon_{min}, R_\epsilon]$, with length $L_1 = R_\epsilon - \epsilon_{min}$ for the first branch of the caustic formation; and along an interval with length L_2 on the second branch of the caustic. By ensuring that $L = L_1 + L_2 = 2R_\epsilon$ for the two branches, the interval for the second branch is $[\epsilon_{min}, R_\epsilon + 2\epsilon_{min}]$. Thus, the averaged number density for scenario **B** is:

$$\hat{n}^p = \frac{1}{2R_\epsilon}\int_{\epsilon_{min}}^{R_\epsilon}\frac{d\delta}{d\epsilon}d\epsilon + \frac{1}{2R_\epsilon}\int_{\epsilon_{min}}^{R_\epsilon+2\epsilon_{min}}\frac{d\delta}{d\epsilon}d\epsilon = \frac{|\delta(R_\epsilon) - \delta_{min}| + |\delta(R_\epsilon + 2\epsilon_{min}) - \delta_{min}|}{2R_\epsilon}\,. \tag{4.3}$$

Finally, introducing the roots $\delta(\pm R_\epsilon) = (-J + \sqrt{J^2 \pm 2HR_\epsilon})/H$ in the expression 4.2 for the scenario **A** and the roots $\delta(R_\epsilon) = (-J + \sqrt{J^2 + 2HR_\epsilon})/H$, $\delta(\epsilon_{min}) = -J/H$ and $\delta(R_\epsilon + 2\epsilon) = (-J + \sqrt{2HR_\epsilon - J^2})/H$ in the equation 4.3 for the scenario **B**, $\hat{n}^p$ averaged on a characteristic length–scale $2R_\epsilon$ is:

$$\hat{n}^p = \begin{cases} \frac{2}{\sqrt{J^2+2HR_\epsilon}+\sqrt{J^2-2HR_\epsilon}} & \text{if } J^2 - 2HR_\epsilon > 0 \\ \frac{\sqrt{J^2+2HR_\epsilon}+\sqrt{-J^2+2HR_\epsilon}}{2R_\epsilon H} & \text{if } J^2 - 2HR_\epsilon < 0\,. \end{cases} \tag{4.4}$$

For $J^2 >> 2HR_\epsilon$, the above expression simplifies to the classical FLA expression $\hat{n}^p = 1/J$.

For the calculation of a scalar magnitude $\mathbf{H}$ for the Hessian, along the primary direction of a caustic filament from H_{ijk}, the angle θ between the coordinate systems that are attached to the fold (i.e. (η, ζ) and (η_0, ζ_0)) in relation to the global coordinates (x, y) and (x_0, y_0) is assumed. The transformation between the two systems for both the initial and the current positions is written as:

$$(\eta, \eta_0) = (x, x_0)\cos\theta + (y, y_0)\sin\theta \ , \ (\zeta, \zeta_0) = -(x, x_0)\sin\theta + (y, y_0)\cos\theta \ , \tag{4.5}$$

$$(x, x_0) = (\eta, \eta_0)\cos\theta - (\zeta, \zeta_0)\sin\theta \ , \ (y, y_0) = (\eta, \eta_0)\sin\theta + (\zeta, \zeta_0)\cos\theta \ . \tag{4.6}$$

Based on the assumption of the one–dimensional structure of the caustic filament the curvature of the DC on the ζ direction can be ignored and the Hessian magnitude $\mathbf{H}$ on the direction ζ can be defined as $H = \frac{\partial^2 \eta}{\partial \eta_0^2}$. In order to evaluate the second derivative, we start from the first derivative which can be written as:

$$\frac{\partial \eta}{\partial \eta_0} = \frac{\partial \eta}{\partial x_0}\frac{\partial x_0}{\partial \eta_0} + \frac{\partial \eta}{\partial y_0}\frac{\partial y_0}{\partial \eta_0} = \frac{\partial x}{\partial x_0}\cos^2\theta + \frac{\partial y}{\partial x_0}\sin\theta\cos\theta + \frac{\partial x}{\partial y_0}\sin\theta\cos\theta + \frac{\partial y}{\partial y_0}\sin^2\theta \ . \tag{4.7}$$

This result is obtained using the transformation equations 4.5 for η and ζ in terms of x and y and the partial derivatives of the Lagrangian coordinates, deduced from 4.6 (i.e. $\frac{\partial x_0}{\partial \eta_0} = cos\theta$ and $\frac{\partial y_0}{\partial \eta_0} = sin\theta$). The second derivative is obtained by differentiating 4.7 on η_0 using the expressions $\frac{\partial x_0}{\partial \eta_0} = cos\theta$ and $\frac{\partial y_0}{\partial \eta_0} = sin\theta$ and also the following evaluations of the chain rule:

$$\frac{\partial}{\partial \eta_0}\left(\frac{\partial x}{\partial x_0}\right) = \frac{\partial^2 x}{\partial x_0 \partial x_0}\frac{\partial x_0}{\partial \eta_0} + \frac{\partial^2 x}{\partial y_0 \partial x_0}\frac{\partial y_0}{\partial \eta_0} \ , \frac{\partial}{\partial \eta_0}\left(\frac{\partial y}{\partial x_0}\right) = \frac{\partial^2 y}{\partial x_0 \partial x_0}\frac{\partial x_0}{\partial \eta_0} + \frac{\partial^2 y}{\partial y_0 \partial x_0}\frac{\partial y_0}{\partial \eta_0}$$

$$\frac{\partial}{\partial \eta_0}\left(\frac{\partial x}{\partial y_0}\right) = \frac{\partial^2 x}{\partial x_0 \partial y_0}\frac{\partial x_0}{\partial \eta_0} + \frac{\partial^2 x}{\partial y_0 \partial y_0}\frac{\partial y_0}{\partial \eta_0} \ , \frac{\partial}{\partial \eta_0}\left(\frac{\partial y}{\partial y_0}\right) = \frac{\partial^2 y}{\partial x_0 \partial y_0}\frac{\partial x_0}{\partial \eta_0} + \frac{\partial^2 y}{\partial y_0 \partial y_0}\frac{\partial y_0}{\partial \eta_0} \ . \tag{4.8}$$

The second derivative $\mathbf{H} = \frac{\partial^2 \eta}{\partial \eta_0^2}$ can be obtained from 4.7 as:

$$\mathbf{H} = H_{111}\cos^3\theta + H_{121}\cos^2\theta\sin\theta + H_{211}\cos^2\theta\sin\theta + H_{221}\cos\theta\sin^2\theta$$

$$+ H_{112}\cos^2\theta\sin\theta + H_{122}\cos\theta\sin^2\theta + H_{212}\cos\theta\sin^2\theta + H_{222}\sin^3\theta \ . \tag{4.9}$$

The primary direction of the fold is calculated by finding the $\theta \in [0 : 2\pi]$ that maximises $\mathbf{H}$ in 4.9. This maximum value $\mathbf{H}$ is used for the evaluation of the number density for a finite volume with radius R_ϵ as dictated by 4.4. The result of this analysis for $\hat{n}^p$ at the instance $t = 0.4$ and $R_\epsilon = 0.001$ is shown in figure 4. It can be observed that this method provides a finite value for $\hat{n}^p$ and the loci of number density maxima corresponds to the caustic formations shown in figure 1.

The orange grid lines in the figures 2(**a-d**) represent the "DC-structure" as described by the "second–order" FLA, assuming this one–dimensional structure, that accounts for the DC curvature along the primary direction only. The Taylor expansion of the Eulerian coordinates (η, ζ), expressed in terms of the Lagrangian coordinates (η_0, ζ_0), across the primary direction θ, is:

$$\eta = J_{1,1}\eta_0 + J_{1,2}\zeta_0 + 0.5\mathbf{H}\eta_0^2, \quad \zeta = J_{2,1}\eta_0 + J_{2,2}\zeta_0 \ , \tag{4.10}$$

where the second derivatives on the ζ direction are assumed to be equal to zero, i.e. $\frac{\partial^2}{\partial \zeta_0^2} = 0$, and also $\frac{\partial^2 \zeta}{\partial \eta_0^2} = 0$. Rotating the above expression by the principal direction angle θ, the "DC-structure" on the x, y plane ($\epsilon_1 = x - x^p$ and $\epsilon_2 = y - y^p$) is expressed

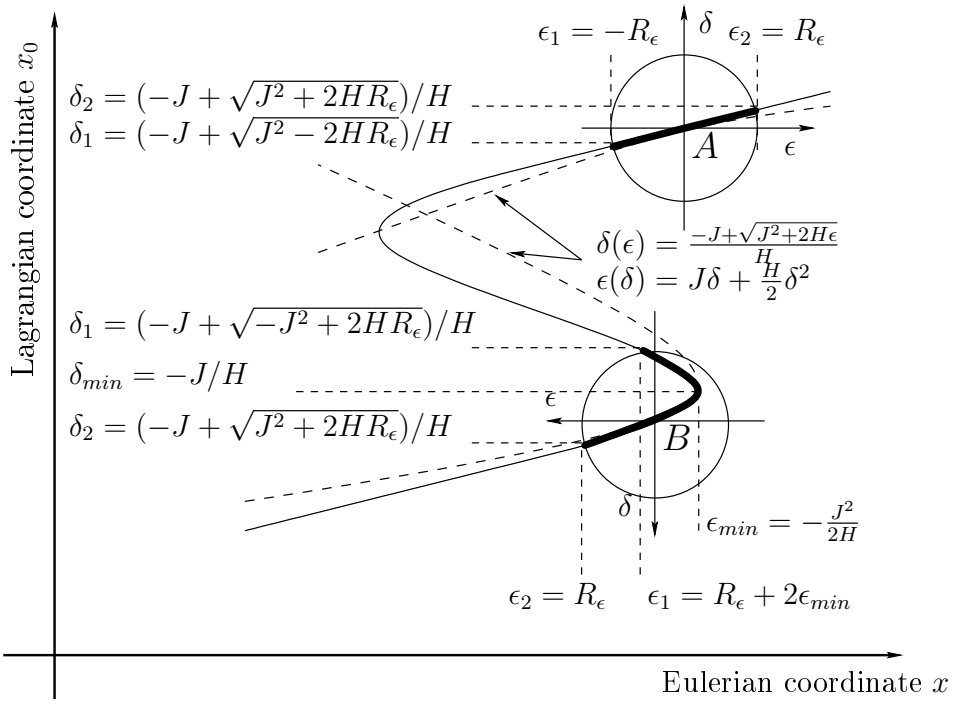


Figure 3: One–dimensional structure of the DC for the scenario **A**:$J^2 - 2HR_\epsilon > 0$ and for the scenario **B**:$J^2 - 2HR_\epsilon < 0$, when the caustic fold occurs within the filtering volume.

as:

$$x - x^p = J_{1,1}\delta_1 + J_{1,2}\delta_2 + 0.5\mathbf{H}\delta_1^2\cos^3\theta + \mathbf{H}\cos^2\theta\sin\theta\delta_1\delta_2 + 0.5\mathbf{H}\cos\theta\sin^2\theta\delta_2^2\ , \quad (4.11)$$

and

$$y - y^p = J_{2,1}\delta_1 + J_{2,2}\delta_2 + 0.5\mathbf{H}\delta_1^2\cos^2\theta\sin\theta + \mathbf{H}\cos\theta\sin^2\theta\delta_1\delta_2 + 0.5\mathbf{H}\sin^3\theta\delta_2^2\ , \quad (4.12)$$

where $\delta_1 = x_0 - x_0^p$ and $\delta_2 = y_0 - y_0^p$.

In figure 5 we present a comparison of the number densities for the reference particle $(-0.05, 0.1)$ calculated using both the standard FLA (using the model 2.1) the "second–order" FLA (4.1), and the "second–order" FLA using a one–dimensional structure for the DC (see equations 4.4 and 4.9) , compared to the result inferred from the direct numerical integration of particle trajectories using 4.1.

In order to calculate all densities from the various models and compare them to the LA result, at a consistent length scale, the analytical model described by 4.4 is evaluated at a length scale R_ϵ which is inferred from the LA simulation. R_ϵ shown in the figure 3 corresponds to the length–scale of the caustic formation across the agglomeration front. The deformed DC on a caustic is a strongly anisotropic filament and is characterised by a maximum and a minimum length, namely R_{max} and R_{min} respectively. An estimate for the thickness of this caustic filament R_ϵ can be obtained from R_{min}. Given that we know the surface of the caustic S_t the minimum length–scale that corresponds to the deformed caustic can be calculated from R_{max} as $R_{min} = S_t/(4R_{max})$. Thus an estimate for R_ϵ is: $R_\epsilon = S_t/(4R_{max})$.

As it can be inferred from figure 5(**a**), all approaches predict the number density as calculated by the direct integration of a dense cloud of particle trajectories using the

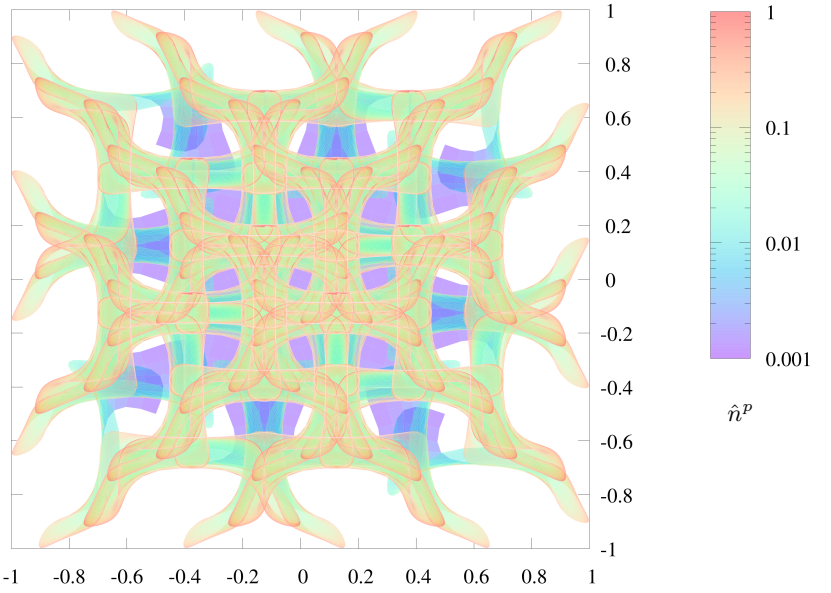


Figure 4: Instance $t = 0.4$, represented as a deformed DC. The gradient of the surface identifies the caustic formations and its curvature is related to the intensity of the caustics. The surface is coloured by $\hat{n}^p$, with $R_\epsilon = 0.001$. $St = 0.1$.

standard LA for almost the whole interval of the simulation. At the instance $t \sim 0.1655$, however, and for a duration of $\Delta t \sim 0.001$, the reference particle goes through a caustic. The performance of the approaches presented close to the caustic is shown in detail in figure 5(**b**). As expected, the first–order FLA identifies the caustic as a singularity point. The "second–order" FLA succeeds in calculating the number density accurately, by predicting the particle distribution as shown in figure 2(**b**). The one–dimensional analytical model for $\hat{n}^p$ expressed by 4.4, also predicts the occurrence and the intensity of the caustic for $R_\epsilon = S_t/(4R_{max})$. Additionally, the result of the same model is shown for a constant $R_\epsilon = 3.5 \cdot 10^{-6}$. This is the minimum length scale observed during the singularity. As can be inferred from 5(**b**), the choice of R_ϵ affects the identification of the onset of the caustic. The length–scale $R_\epsilon = S_t/(4R_{max})$ is larger before and after the singularity thus the time interval of the caustic is over predicted. When using the constant length–scale $R_\epsilon = 3.5 \cdot 10^{-6}$ the predicted period for the caustic is closer to the one calculated by the other methods. As the LA simulation progresses in time, the neighbours of the reference particle eventually diverge significantly and their motion becomes uncorrelated. This results to the divergence of the results calculated by the Fully Lagrangian methods, to the result calculated by the standard LA, after $t = 0.4$ (see figure 5).

5. Particle structure for different Stokes numbers

In figure 6 density distributions for the KS of 250000 particles transported by the Taylor vortex field described in 3.1 are presented for two different Stokes numbers (i.e. $St = 0.001$ and $St = 0.01$). The result for $St = 0.1$ is shown in the figure 4. Although the particles manage to escape the vortices of the carrier phase flow field for the higher Stokes number case (see figure 4), this is not the case for the lower St number simulations. From the figure 6 it can be inferred that for the smallest and intermediate Stokes numbers (i.e. $St = 0.001$

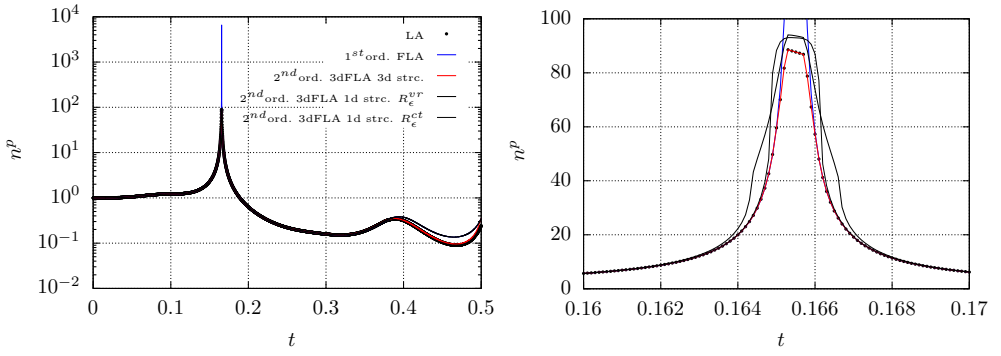


Figure 5: Number density $\hat{n}^p$ along the reference particle trajectory. Black circles: Direct integration (LA). Blue curve: standard FLA. Red curve: result inferred from the "second–order" continuum structure. Black curve: Second order FLA analytical model for one–dimensional "DC-structure" assuming a variable predicted filtering width $R_\epsilon^{vr} = S_t/(4R_{max})$. Thin black curve: Second order FLA analytical model for one–dimensional "DC-structure" assuming a cosntant filtering width that corresponds to the R_ϵ^{var} on the caustic $R_\epsilon ct = 3.5 \cdot 10^{-6}$. **a**: $t = 0 - 0.5$. **b**: $t = 0.16 - 0.17$.

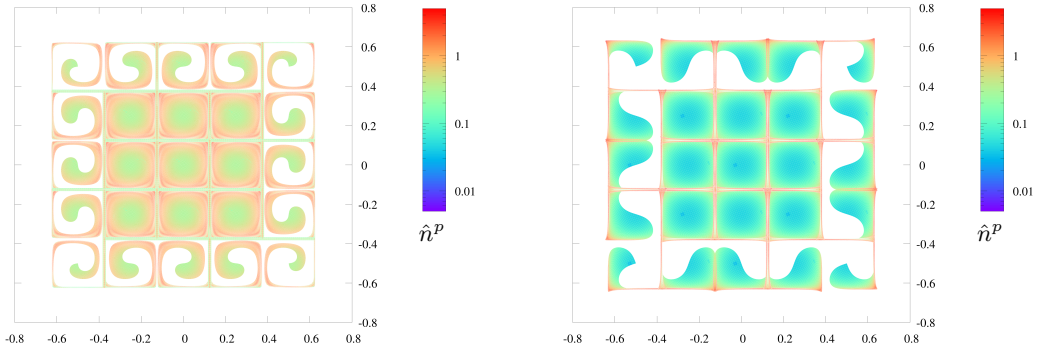


Figure 6: Instance $t = 0.4$, represented as a deformed DC. The surface is coloured by $\hat{n}^p$, with $R_\epsilon = 0.001$. **a**: $St = 0.001$. **b**: $St = 0.01$.

and $St = 0.01$) the particles do not escape the bounds of their initial distribution and remain trapped within the Taylor vortices. In the same figure 6 we can observe that for $St = 0.001$ the particles follow the carrier phase velocity field. They asymptotically reach the bounds of each Taylor vortex to agglomeration regions at the positions of high shear. For the intermediate Stokes numbers, though, the particles undulate across the shear layer to neighbouring vortical cells but they still remain engulfed within the vortices. In both cases though, it is evident that strong caustics form at the boundary of each vortex.

In the figures 7 to 9 we present the ensemble average $< \cdot >= \frac{1}{N}\sum_{i=1,N}(\cdot)$ of the number density for the three different KS (i.e. $St = 0.001$, $St = 0.01$ and $St = 0.1$). For the lowest Stokes number case, shown in the figure 7 the point-wise number density

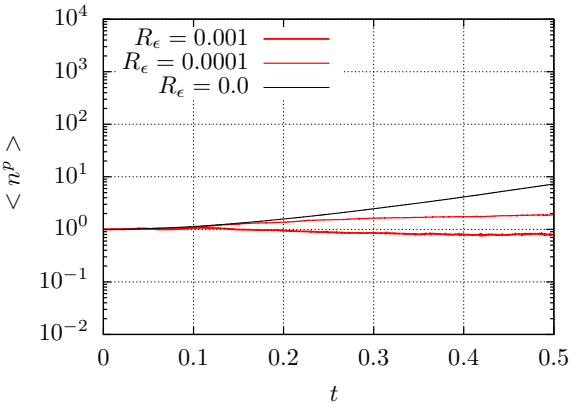


Figure 7: Evolution of number density $\hat{n}^p$ averaged at different length scales, compared with the standard FLA number density $1/\mathbf{J}$. Black curve: Standard FLA $R_\epsilon = 0$. Thin red curve: "second–order" FLA with $R_\epsilon = 0.0001$. Thick red curve: "second–order" FLA with $R_\epsilon = 0.001$. Results for $St = 0.001$.

presents no evidence of singularities and crossing trajectories and the averaged point-wise density increases monotonically in time. The averaged density defined at finite length scales (i.e. $R_\epsilon = 0.0001$ and $R_\epsilon = 0.001$), though reaches a constant level after $t = 2.5$. For the intermediate Stokes number case $St = 0.01$, shown in the figure 8, the point-wise number density presents intense spikes due to singularities related to crossing trajectories. It can be inferred from the figure 6 that caustics appear at the boundaries of the vortices (see Chen *et al.* (2006)), for both the low and the intermediate Stokes number cases. In the first case though, the agglomeration is achieved by particles that reach the edge of each vortex in an asymptotic manner. For the intermediate Stokes number, however, the particles undulate across the vortex boundaries presenting crossing trajectories. Thus, it can be deduced that the instances of $J = 0$ cannot be perceived as sufficient criteria for the formation of caustics. The accumulation of particles in caustics is rather characterised by the number density value, which provides a measure for the intensity of the caustic.

The actual values of the spikes in the first–order FLA number density are spurious and coincidental. These values are dependent on the temporal resolution of the integration of the initial value problem in 2.10 during the change of sign of the Jacobian. Nevertheless, the average point-wise density is monotonically increasing in time. The average density defined at finite length–scales (i.e. $R_\epsilon = 0.0001$ and $R_\epsilon = 0.001$) though, reaches a constant value after $t = 0.1$. The evolution of the filtered number densities to a constant value can be attributed to the length scale of the caustics becoming smaller than the filtering length R_ϵ. From that critical point and onward the focusing effect of the flow on the particle distribution is filtered out. Given that for both cases the particles remain within a constant volume, the averaged number density remains constant. For the higher Stokes number configuration the particles have enough inertia to sling out the eddies, thus, the DC is expanding in time resulting to the gradual reduction of the average number density.

The filtering effect stemming out of the definition of a number density for a finite length–scale is presented in the figure 10. In this figure the Probability Density Function (PDF) for the number density at $t = 0.4$ for the $St = 0.1$ KS is shown. The filtering operator $\hat{(\cdot)}$ is cutting off the higher instances of the number density which affect the symmetry of the number density PDF (Meneguz & Reeks 2011; Fessler *et al.* 1994).

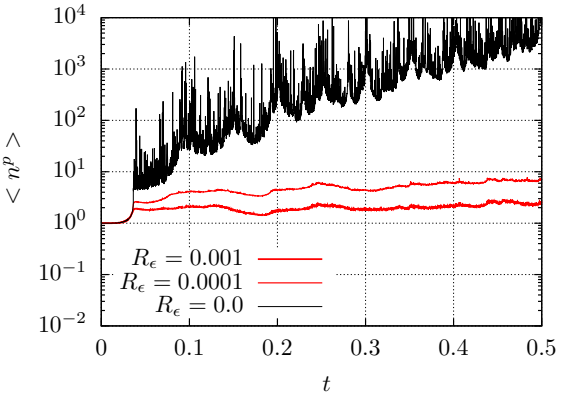


Figure 8: Evolution of number density $\hat{n}^p$ averaged at different length scales, compared with the standard FLA number density $1/J$. Black curve: Standard FLA $R_\epsilon = 0$. Thin red curve: "second–order" FLA with $R_\epsilon = 0.0001$. Thick red curve: "second–order" FLA with $R_\epsilon = 0.001$. Results for $St = 0.01$.

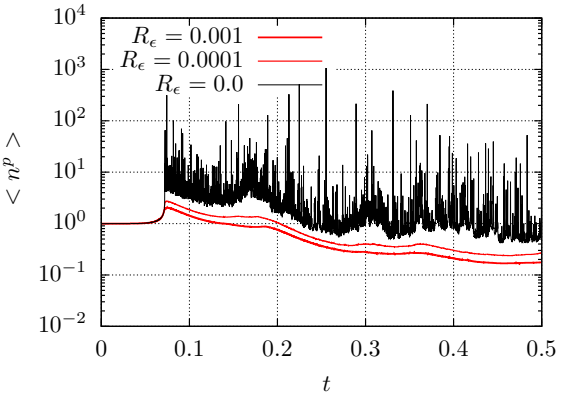


Figure 9: Evolution of number density $\hat{n}^p$ averaged at different length scales, compared with the standard FLA number density $1/J$. Black curve: Standard FLA $R_\epsilon = 0$. Thin red curve: "second–order" FLA with $R_\epsilon = 0.0001$. Thick red curve: "second–order" FLA with $R_\epsilon = 0.001$. Results for $St = 0.1$.

6. Discussion

Equation 4.10 can provide an estimate of the interparticle distance given an initial particle separation $\Delta\delta$. The result for the reference particle studied in the previous Section, is presented in the figure 11 for three different levels of initial particle loading $\Delta\delta = 0.01, 0.001$ and 0.0001. As it can be inferred from the equation 4.10, the interparticle distance is not necessarily zero on the caustic but proportional to the Hessian magnitude $\mathbf{H}$ (i.e. $\Delta\epsilon = 1/2\mathbf{H}\,(\Delta\delta)^2$). It can be observed that for low initial loadings (e.g. $\Delta\delta = 0.01$) the decrease of the interparticle distance is less than one order of magnitude which can be well above the particles size. At this point we need to highlight the differences between the dispersed continuum (DC) and the particulate phase. We suggest that although the dispersed continuum can overlap with itself, the particles (or droplets) do not need to. The reason for this is that although the DC is continuous, the particulate phase is not.

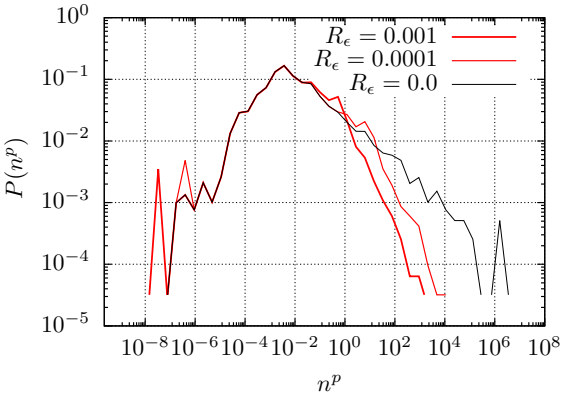


Figure 10: Probability density function for the number density distribution at $t = 0.4$ for the $St = 0.1$ case. Black curve: Standard FLA $R_\epsilon = 0$. Thin red curve: "second–order" FLA with $R_\epsilon = 0.0001$. Thick red curve: "second–order" FLA with $R_\epsilon = 0.001$.

The particles are dispersed and the DC is the continuous Lagrangian space upon which the particles are attached. Thus, the DC being an immaterial entity (i.e. a Lagrangian space), it can fold and intersect itself, resulting to multiply defined layers where multiple velocities can be attributed for each one of the folds at the same Eulerian point.

It is evident that the occurrence of caustics can be identified by the standard FLA (see (Gustavsson & Mehlig 2016)). The standard FLA though, cannot provide a prediction of the number density on the caustic. Furthermore, the spurious values close to the caustic and on the singularity itself, infect analyses based on the standard FLA (Picciotto *et al.* 2005). For example, the number density gradients needed for the closure of the turbulent diffusion as described in the model of Papoutsakis *et al.* (2018*a*) are affected by the FLA singularities. Furthermore, the study of the compressibility of the dispersed continuum and the temporal evolution of the number density in Meneguz & Reeks (2011) is also affected by the occurrence of singularities. Clipping these values results to an indeterminacy of the actual value. Limiting the FLA solution to the value that corresponds to the physical size of the particles or droplets is a rational practice, although, this is not necessary for the "second—order" FLA where the interparticle distances are finite as exhibited in the figure 11.

In Ravichandran & Govindarajan (2015) particle collisions have been related to caustics due to the increased number density and to opposing velocities, thus it is likely for particles belonging to different folds to collide (Wilkinson & Mehlig 2005; Wilkinson *et al.* 2007), and this can happen at any part of the domain where the DC is multiply folded (see Wilkinson *et al.* (2007)). Taking into account the dispersed continuum assumption, the particulate velocity field on a fold is continuous (and differentiable), Lagrangian neighbours have similar velocities (Papoutsakis *et al.* 2018*a*) (i.e. $lim_{\Delta x_0 \to 0} (V(x_0 + \Delta \mathbf{x}_0, t)) = \mathbf{V}(\mathbf{x}_0, t)$). Thus, a collision among Lagrangian neighbours in a caustic is less likely than among particles belonging to overlapping folds.

Here, we present an extension of the FLA that actually predicts the "DC-structure" and does not degenerate in the event of the formation of a caustic. The "second–order" description of the dispersed structure presented in this paper (see 2.4) and depicted by the red mesh in the figure 2(**a-d**) shows an excellent agreement with the direct integration of discrete particles. Gustavsson & Mehlig (2016) and Gustavsson *et al.* (2012) relate the clustering by caustics to a "catastrophe in mathematical terms" as described in Arnold

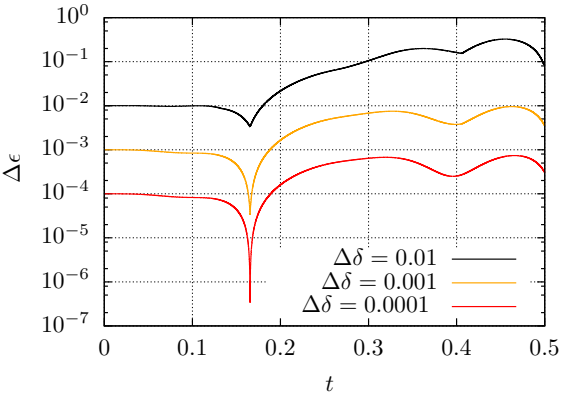


Figure 11: Estimated average inter-particle distance evolution in time for three different particle loads. Black curve: $\Delta\delta = 0.01$. Orange curve:$\Delta\delta = 0.001$. Red curve: $\Delta\delta = 0.0001$.

(1992). Picciotto *et al.* (2005) justifies the infinite number density as a singularity in a mathematical sense. Here, we lift the fold singularity by acknowledging the overlapping of the dispersed phase folds which is inevitable in a pressureless continuum (Papoutsakis *et al.* 2018*a*). Thus we do not believe that the infinite number density occurs because the collisions of the particulate medium are not accounted, they occur at a small length scale lower than the limit of the continuity assumption. The infinite number density is related to the deformation of the DC itself and does not correspond to the number density of the dispersed particles. It is alleviated by defining the number density at a finite length scale using models that account for the curvature of the DC structure.

The method presented can be implemented for carrier phase flow fields inferred either from computational simulations or by experimental data. It needs to be stressed, however, that both the first $\partial U_i/\partial x_j$ and the second $\partial^2 U_i/\partial x_j \partial x_k$ derivatives need to be obtained at the same levels of accuracy as the velocity field $\mathbf{U}(\mathbf{x}, t)$. An approach like this could be used to provide insight for dispersed environmental flows (Lebreton *et al.* 2018) characterised by small particle loading which makes the identification of caustics a challenging task. An LA would need long computational times on a statistically significant number of individual particles.

The length scale $R_\epsilon = S_t/(4R_{max})$ derives from the assumption of a one–dimensional compression of the dispersed phase across the caustic filaments. This is in agreement with the observation of Gustavsson & Mehlig (2016) for the "small scale clustering" of filamentary structures much smaller than the Kolmogorov scales. Although, the dispersed phase exhibits length–scales that are not related to the carrier phase flow-field, in our model, the intensity of the caustics is the result of the integration of the carrier phase flow field history as seen by the particle. This is described by the model equation 4.4. In this equation, the model introduces the effect of the carrier phase velocity and its first derivative (standard FLA) and also introduces the effect of the second spatial derivative of the carrier phase velocity. The effect of the curvature of the carrier phase flow field for the agglomeration of droplets and the segregation of droplets with various sizes has been investigated in Pinsky & Khain (1997).

The relation between the Stokes number of a dispersed flow and the temporal evolution of the averaged first moment for the number density has been expressed by the

proportionality coefficient γ as (Meneguz & Reeks 2011; Ijzermans *et al.* 2010) :

$$< n^d > \propto e^{\gamma t} \ . \tag{6.1}$$

For flows that do not exhibit crossing trajectories (low Stokes numbers) it was found that γ varies with the Stokes number. For higher Stokes numbers, though, it was reported that the intermittent events of infinite number density dominate the statistics (see Ijzermans *et al.* (2010)) so this analysis was not extended for higher Stokes numbers. In Meneguz & Reeks (2011) the negative compressibility was attributed to the effect of the singularities. The introduction of the zeroth moment did not augment the understanding of the evolution of the number density since the zeroth moment results in a degeneration of FLA to a standard Lagrangian method (LA). For flows that do exhibit caustics (high Stokes numbers), the frequency of caustic instances was studied instead of the number density. The frequency of singularity events was chosen as a measure of the accumulation of particles in a dispersed flow, since the FLA number density was infected by singularities (Gustavsson *et al.* 2012). The finite length–scale number density, though, shown in the figures 7 to 9 is not affected by singularities. In our case the proportionality coefficient γ is related to the expansion of the DC and exhibits a simpler behaviour. Specifically, for the low Stokes numbers an invariable averaged number density is identified due to the fact that the DC cannot escape the vortices. For the higher Stokes number case, which results to a monotonically expanding DC, the average number density reduces, thus implying negative values for γ.

In the analysis presented here it became evident that caustics are not necessarily related to singularities in $1/J$. The singularities identify crossing trajectories which result to high spurious number densities. High number densities were also achieved by the gradual agglomeration of particles as shown for the low Stokes number KS. This is in agreement to the multiple mechanisms for the formation of caustics documented in Gustavsson & Mehlig (2016). Thus, it can be deduced that the instances of $J = 0$ cannot be perceived as sufficient criteria for the formation of caustics. The accumulation of particles to caustic formations is rather characterised by the actual value of the number density itself.

The standard LA needs three kinematic equations for each direction and three momentum equations for the particle velocity resulting to six (6) equations per particle. FLA instead demands 9 more equations for the Jacobian entries and 9 the corresponding rates of the Jacobian, i.e. twenty-four (24) ODE's in total. For the "second–order" FLA in three dimensions 78 ODE's need to be solved. Thus, the computational cost for the FLA is four times bigger than an LA and for the "second–order" FLA it is 13 times more than the LA. However, we must keep in mind that the FLA approaches do not need an exhaustive number of representative particles to obtain the number density. FLA and "second—order" FLA provide a particle/droplet number density by solving of the mass conservation in a Lagrangian formulation and not by integration of a statistically significant number of representative particles as in the standard Lagrangian Approach (LA).

The suggested extended approach presents a wide applicability, since the added features do not impose extra computational restrictions that would narrow down its implementation range in relation to the standard Lagrangian approaches. The current formulation can be applied to particles transporting under a drag force that is related to the particle-carrier phase slip velocity including the Stokes drag case investigated in this work.

The importance of the introduction of a length scale in the definition of the number density is emphasised in Monchaux *et al.* (2012), where the identification of particle clustering was based on the relation of the number density to the length–scale of the averaging volume on which the number density is defined. Here, an explicit relation

between the density of the dispersed phase to the length on which the number density is defined has been presented and the relation between the temporal evolution of the averaged number density for higher Stokes numbers was investigated. The number density was linked to a finite length scale on a robust analytical framework that highlights the physics of the formation of the caustics and explains the causes of the resulting singularities. This framework is needed for the introduction of the FLA to turbulent flows in the LES context (Papoutsakis *et al.* 2018*a*). The identification of the structure of caustics presented in this work paves the way to a robust understanding of the mechanisms which induce caustics from the "second–order" structure of the carrier phase flow field (Marchioli 2017).

One important impact of the "second–order" FLA and the solution for a number density defined on a given length scale is that it can be coupled with the filtered flow fields. FLA has been subject to criticism in Ravichandran & Govindarajan (2015), because it accounts for the carrier phase velocity gradients at the locality of the reference particle (e.g. in geophysical flows). For flows with high Reynolds numbers the Kolmogorov scale can be much smaller that the interparticle distance. Thus, the apparent drift velocity among Lagrangian neighbours is not correlated. Filtering the turbulent flow field, however, allows for accounting only for the large coherent vortical structures while the effect of the remaining filtered unresolved smaller scales can then be accounted for by a diffusion model as in Papoutsakis *et al.* (2018*a*).

Infinite number density has been related to trajectory crossings (Healy & Young 2005). However, we understand that trajectory crossings are related to the DC rather that the particles as such, since they are attached to the DC in a dispersed manner with finite non-zero interparticle separation. Thus, the fact that the DC continuum may overlap it does not necessarily mean that the particles are overlapping too.

7. Conclusion

Caustics are characterised by the compression of the dispersed phase to a fine scale, thus their identification using Lagrangian methods demands an exhaustive number of representative particles. The standard FLA succeeds in identifying caustics, but results in singular values for the number density. In this work, we present the derivation of an original method which predicts the "second–order" "DC-structure". This method is a "second–order" extension of the FLA that can identify and quantify the occurrence and intensity of caustics. The model requires only one trajectory for the calculation of the particulate number density, by integrating the Jacobian and the Hessian of the transformation from the Lagrangian to the Eulerian coordinates using information from the carrier phase velocity field and its first and second spatial derivatives. Number density is calculated from the "DC–structure", either numerically from the deformed DC, or by a novel analytical model which assumes a one–dimensional structure. Furthermore, the integrability of the point-wise number density of the FLA approach was exhibited. The model presented relates the FLA number density to a finite length scale Δ needed for the introduction of the FLA to turbulent flows. The identification of the "DC-structure" of caustics presented in this work paves the way to a robust understanding of the mechanisms which induce caustics from the "second–order" structure of the carrier phase flow field.

REFERENCES

Arnold, V.I. 1992 *Catastrophe Theory*. Berlin: Springer.

Bec, J. 2003 Fractal clustering of inertial particles in random flows. *Physics of Fluids* **15** (11), arXiv: 0306049.

Bell, M.L., Dominici, F., Ebisu, K., Zeger, S. L. & Samet, J.M. 2007 Spatial and temporal variation in pm2.5 chemical composition in the united states for health effects studies. *Environmental Health Perspectives* **115** (7), 989–995.

Chen, L., Goto, S. & Vassilicos, J.C. 2006 Turbulent clustering of stagnation points and inertial particles. *J. Fluid Mech.* **553**, 143–154.

Crisanti, A., Falcioni, M., Provenzale, A., Tanga, P. & Vulpiani, A. 1992 Dynamics of passively advected impurities in simple two-dimensional flow models. *Physics of Fluids A* **4** (8), 1805–1820.

Ducasse, L. & Pumir, A. 2009 Inertial particle collisions in turbulent synthetic flows: Quantifying the sling effect. *Phys. Rev. E* **80**, 066312.

Fessler, J. R., Kulick, J. D. & Eaton, J. K. 1994 Preferential concentration of heavy particles in a turbulent channel flow. *Physics of Fluids.* **6** (11), 3742–3749.

Gustavsson, K. & Mehlig, B. 2016 Statistical models for spatial patterns of heavy particles in turbulence. *Advances in Physics* **65** (1), 1–57.

Gustavsson, K., Meneguz, E., Reeks, M.W. & Mehlig, B. 2012 Inertial-particle dynamics in turbulent flows: caustics, concentration fluctuations and random uncorrelated motion. *New Journal of Physics* **14**.

Healy, D.P. & Young, J.B. 2005 Full Lagrangian methods for calculating particle concentration fields in dilute gas-particle flows. *Proceedings of the Royal Society of London A: Mathematical, Physical and Engineering Sciences* **461** (2059), 2197–2225.

Ijzermans, R.H.A., Meneguz, E. & Reeks, M.W. 2010 Segregation of particles in incompressible random flows: singularities, intermittency and random uncorrelated motion. *J. Fluid Mech.* **653**, 99–136.

Ijzermans, R.H.A., Reeks, M.W., Meneguz, E., Picciotto, M. & Soldati, A. 2009 Measuring segregation of inertial particles in turbulence by a full Lagrangian approach. *Phys. Rev. E* **80**, 015302.

Kasbaoui, M.H., Koch, D.L. & Desjardins, O. 2019 Clustering in Euler-Euler and Euler-Lagrange simulations of unbounded homogeneous particle-laden shear. *Journal of Fluid Mechanics* **859**, 174–203.

Knight, G. 2012 *Plastic pollution.* Chicago, Ill. :: Heinemann Library.

Lebreton, L., Slat, B., Ferrari, F., Sainte-Rose, B., Aitken, J., Marthouse, R., Hajbane, S., Cunsolo, S., Schwarz, A., Levivier, A., Noble, K., Debeljak, P., Maral, H., Schoeneich-Argent, R., Brambini, R. & Reisser, J. 2018 Evidence that the Great Pacific Garbage Patch is rapidly accumulating plastic. *Scientific Reports* **8** (1).

Marble, F.E. 1970 Dynamics of dusty gases. *Ann. Rev. Fluid Mech.* **2** (1), 397–446.

Marchioli, C. 2017 Large-eddy simulation of turbulent dispersed flows: a review of modelling approaches. *Acta Mechanica* **228** (3), 741–771.

Meneguz, E. & Reeks, M.W. 2011 Statistical properties of particle segregation in homogeneous isotropic turbulence. *J. Fluid Mech.* **686**, 338–351.

Monchaux, R., Bourgoin, M. & Cartellier, A. 2012 Analyzing preferential concentration and clustering of inertial particles in turbulence. *International Journal of Multiphase Flow* **40**, 1 – 18.

Osiptsov, A.N. 1984 Investigation of regions of unbounded growth of the particle concentration in disperse flows. *Fluid Dynamics* **19** (3), 378–385.

Papoutsakis, A., Rybdylova, O.D., Zaripov, T.S., Danaila, L., Osiptsov, A.N. & Sazhin, S.S. 2018*a* Modelling of the evolution of a droplet cloud in a turbulent flow. *Int. J. Multiph. Flow* **104**, 233–257.

Papoutsakis, A., Sazhin, S.S., Begg, S., Danaila, I. & Luddens, F. 2018*b* An efficient Adaptive Mesh Refinement (AMR) algorithm for the Discontinuous Galerkin method: Applications for the computation of compressible two-phase flows. *J. Comput. Phys.* **363**, 399–427.

Picciotto, M., Marchioli, C., Reeks, M.W. & Soldati, A. 2005 Statistics of velocity and preferential accumulation of micro-particles in boundary layer turbulence. *Nuclear Engineering and Design* **235** (10–12), 1239 – 1249.

Pinsky, M.B. & Khain, A.P. 1997 Turbulence effects on droplet growth and size distribution in clouds–A review. *J. Aerosol Sci.* **28** (7), 1177–1214.

Ravichandran, S. & Govindarajan, R. 2015 Caustics and clustering in the vicinity of a vortex. *Physics of Fluids* **27** (3), arXiv: 1503.06919.

Rygg, A., Hindle, M. & Longest, P.W. 2016 Linking Suspension Nasal Spray Drug Deposition Patterns to Pharmacokinetic Profiles: A Proof-of-Concept Study Using Computational Fluid Dynamics. *Journal of Pharmaceutical Sciences* **105** (6), 1995–2004.

Sazhin, S.S. 2014 *Droplets and Sprays*. London: Springer.

Serrano, X.M., Baums, I.B., Smith, T.B., Jones, R.J., Shearer, T.L. & Baker, A.C. 2016 Long distance dispersal and vertical gene flow in the Caribbean brooding coral Porites astreoides. *Sci. Rep.* **6** (1), 21619.

Thomas, A.J. & Martin, J.M. 1986 First assessment of Chernobyl radioactive plume over paris. *Nature* **321**, 817–819.

Tomita, K. & Den, M. 1986 Gauge-invariant perturbations in anisotropic homogeneous cosmological models. *Physical Review D* **34** (12), 3570–3583.

Vogel, S. 1994 *Life in moving fluids : the physical biology of flow*. Princeton University Press.

Wilkinson, M. & Mehlig, B. 2005 Caustics in turbulent aerosols. *Europhysics Letters (EPL)* **71** (2), 186–192.

Wilkinson, M., Mehlig, B., Östlund, S. & Duncan, K.P. 2007 Unmixing in random flows. *Physics of Fluids* **19** (11), arXiv: 0612061.

Williams, F.A. 1958 Spray combustion and atomization. *Physics of Fluids* **1** (6), 541–545.